Geosci. Model Dev. Discuss., 8, 2847–2873, 2015
www.geosci-model-dev-discuss.net/8/2847/2015/
doi:10.5194/gmdd-8-2847-2015
© Author(s) 2015. CC Attribution 3.0 License.

Geoscientific Model Development Discussions
Open Access

This discussion paper is/has been under review for the journal Geoscientific Model Development (GMD). Please refer to the corresponding final paper in GMD if available.

An analytical verification test for numerically simulated convective flow above a thermally heterogeneous surface

A. Shapiro[1,2], **E. Fedorovich**[1], **and J. A. Gibbs**[1]

[1]School of Meteorology, University of Oklahoma, Norman, Oklahoma, USA
[2]Center for Analysis and Prediction of Storms, University of Oklahoma, Norman, Oklahoma, USA

Received: 7 January 2015 – Accepted: 18 February 2015 – Published: 16 March 2015

Correspondence to: A. Shapiro (ashapiro@ou.edu)

Published by Copernicus Publications on behalf of the European Geosciences Union.

Abstract

An analytical solution of the Boussinesq equations for the motion of a viscous stably stratified fluid driven by a surface thermal forcing with large horizontal gradients (step changes) is obtained. The solution can be used to verify that computer codes for Boussinesq fluid system simulations are free of errors in formulation of wall boundary conditions, and to evaluate the relative performances of competing numerical algorithms. Because the solution pertains to flows driven by a surface thermal forcing, one of its main applications may be for testing the no-slip, impermeable wall boundary conditions for the pressure Poisson equation. Examples of such tests are presented.

1 Introduction

Thermal disturbances associated with variations in underlying surface properties can drive local circulations in the atmospheric boundary layer (Atkinson, 1981; Briggs, 1988; Hadfield et al., 1991; Segal and Arritt, 1992; Simpson, 1994; Mahrt et al., 1994; Pielke, 2001; McPherson, 2007; Kang et al., 2012) and affect the development of the convective boundary layer (Patton et al., 2005; van Heerwaarden et al., 2014). Computational fluid dynamics (CFD) codes for modeling such flows commonly solve the Boussinesq equations of motion and thermal energy for a viscous/diffusive stably stratified fluid. In this paper we present an analytical solution of the Boussinesq equations for flows driven by a surface thermal forcing with large gradients (step changes) in the horizontal. The solution can be used to verify that CFD codes for Boussinesq fluid system simulations are free of errors, and to evaluate the relative performances of competing numerical algorithms. Such verification procedures are important in the development of CFD models designed for research, operational, and classroom applications.

We solve the linearized Navier–Stokes and thermal energy equations analytically for the case where the surface buoyancy varies laterally as a square wave (Fig. 1). Attention is restricted to the steady state. No boundary-layer approximations are made; the

GMDD
8, 2847–2873, 2015

solution is non-hydrostatic, and both horizontal and vertical derivatives are included in the viscous stress and thermal diffusion terms. The solution is similar to that of Axelsen et al. (2010) for katabatic flow above a cold strip, but is easier to evaluate (no slope present) and applies to the more general scenario where the viscosity and diffusivity coefficients can differ. The linearized Navier–Stokes equations apply to a class of very low Reynolds number motions known as creeping flows. Such flows appear in studies of lubrication, locomotion of microorganisms, lava flow, and flow in porous media. Of course, for the task at hand, if our linear solution is to serve as a benchmark for a nonlinear numerical model solution, it is essential that the parameter space be restricted to values for which the model's nonlinear terms are negligible.

Because the solution pertains to flows driven by a surface thermal forcing, one of its main applications may be as a test for surface boundary conditions in the pressure Poisson equation. In models of atmospheric boundary layer flows, the buoyancy is a major contributor to the forcing term in the Poisson equation and also appears in the associated surface boundary condition. The pressure boundary condition on a solid boundary in incompressible (Boussinesq) fluid flows is an important and complex issue that has long been fraught with technical difficulties and controversies (Strikwerda, 1984; Orszag et al., 1986; Gresho and Sani, 1987; Gresho, 1990; Temam, 1991; Henshaw, 1994; Petersson, 2001; Sani et al., 2006; Rempfer, 2006; Guermond et al., 2006; Nordström et al., 2007; Shirokoff and Rosales, 2011; Hosseini and Feng, 2011; Vreman, 2014). Typical fractional-step solution methodologies and associated pressure (or pseudo-pressure) boundary-condition implementations are often verified using various prototypic flows such as Poiseuille flows, lid-driven cavity flows, flows over cylinders or bluff bodies, viscously decaying vortices, and dam-break flows. We are unaware of verification tests in which flows were driven by a heterogeneous surface buoyancy forcing. Our solution is designed to fill this gap.

The analytical solution is derived in Sect. 2. In Sect. 3, this solution is compared to numerically simulated fields in a steady state. Two versions of a numerical code are run: a version in which the correct surface pressure boundary condition is applied,

GMDD
8, 2847–2873, 2015

and a version in which the pressure condition is mis-specified. A summary follows in Sect. 4.

2 Analytical solution

We derive the solution for steady flow over an underlying surface along which the buoyancy varies laterally as a single harmonic function. This single-harmonic solution is then used as a building block in a Fourier representation of the square-wave solution.

2.1 Governing equations

Consider the flow of a viscous stably stratified fluid that fills the semi-infinite domain above a solid horizontal surface (placed at $z = 0$). This surface undergoes a steady thermal forcing that varies periodically in the right-hand Cartesian x direction, but is independent of the y direction. The two-dimensional (x, z) flow fields are periodic in x, and satisfy the linearized (assuming the disturbance is of small amplitude) Boussinesq equations,

$$0 = -\frac{\partial \Pi}{\partial x} + \nu \nabla^2 u, \tag{1}$$

$$0 = -\frac{\partial \Pi}{\partial z} + b + \nu \nabla^2 w, \tag{2}$$

$$0 = -N^2 w + \alpha \nabla^2 b, \tag{3}$$

$$\frac{\partial u}{\partial x} + \frac{\partial w}{\partial z} = 0. \tag{4}$$

Here u and w are the horizontal (x) and vertical (z) velocity components, $\Pi \equiv [p - p_e(z)]/\rho_w$ is the kinematic pressure perturbation [p is pressure, $p_e(z)$ is pressure in a hydrostatic environmental state in which the density profile is $\rho_e(z)$, ρ_w is a constant reference density, say, $\rho_e(0)$], and $b \equiv -g[\rho - \rho_e(z)]/\rho_w$ is the buoyancy, where ρ is the

GMDD
8, 2847–2873, 2015

actual density, and g is the acceleration due to gravity. The Brunt–Väisälä frequency $N \equiv \sqrt{-(g/\rho_w)\mathrm{d}\rho_e/\mathrm{d}z}$, kinematic viscosity ν, and thermal diffusivity α are taken constant.

We obtain our solution using a standard vorticity/streamfunction formulation. Cross-differentiating Eqs. (1) and (2) yields the vorticity equation,

$$0 = -\frac{\partial b}{\partial x} + \nu\nabla^2\eta, \tag{5}$$

where $\eta \equiv \partial u/\partial z - \partial w/\partial x$ is the vorticity. Eliminating b from Eqs. (3) and (5) yields

$$\nabla^4\eta = \frac{N^2}{\nu\alpha}\frac{\partial w}{\partial x}. \tag{6}$$

Introducing a streamfunction ψ defined through

$$u = \partial\psi/\partial z, \qquad w = -\partial\psi/\partial x, \tag{7}$$

guarantees that Eq. (4) is satisfied, and transforms Eq. (6) into a single equation for ψ,

$$\nabla^6\psi + \frac{N^2}{\nu\alpha}\frac{\partial^2\psi}{\partial x^2} = 0. \tag{8}$$

The dependent variables are assumed to vanish far above the surface ($z \to \infty$). On the surface we apply no-slip ($u = 0$) and impermeability ($w = 0$) conditions, and specify a periodic (in x) buoyancy distribution. As we will now see, restricting the dependent variables to steady periodic forms that vanish as $z \to \infty$ also restricts acceptable distributions of the surface buoyancy. Averaging Eq. (3) over one period (using $w = -\partial\psi/\partial x$) yields $\mathrm{d}^2\overline{b}/\mathrm{d}z^2 = 0$, which integrates to $\overline{b} = A + Bz$ ($\overline{b}$ is the average of b; A and B are constants). Taking $b \to 0$ as $z \to \infty$, implies that $\overline{b} \to 0$ as $z \to \infty$, in which case $A = B = 0$, and $\overline{b}(z) = 0$. In particular, at the surface, $\overline{b}(0) = 0$. If a surface distribution $b(x,0)$ violates this condition, the ground acts as a net heat source/sink. In an unsteady model, such a source/sink would force a continually upward-developing disturbance, and a steady state could never be attained.

GMDD
8, 2847–2873, 2015

2.2 Single-harmonic forcing

For a surface buoyancy of the form $b(x,0) \propto \sin kx$, Eq. (3) indicates that ψ is of the form

$$\psi = A(z)\cos kx. \tag{9}$$

Application of Eq. (9) in Eq. (8) yields

$$\left(\frac{\mathrm{d}^2}{\mathrm{d}z^2} - k^2\right)^3 A - \frac{N^2k^2}{\nu\alpha}A = 0, \tag{10}$$

which has solutions of the form $A \propto e^{Mz}$ for M satisfying

$$(M^2 - k^2)^3 = \frac{N^2k^2}{\nu\alpha}. \tag{11}$$

Taking the one-third power of Eq. (11) yields a useful intermediate result:

$$M^2 - k^2 = \frac{N^{2/3}k^{2/3}}{\nu^{1/3}\alpha^{1/3}}e^{2n\pi i/3}, \tag{12}$$

where n is an integer. Rearranging Eq. (12) and taking the square root yields,

$$M = \pm\sqrt{k^2 + \frac{N^{2/3}k^{2/3}}{\nu^{1/3}\alpha^{1/3}}e^{2n\pi i/3}}. \tag{13}$$

Equation (13) furnishes six roots, two for each of $n = 0, 1, 2$. To ensure that $A(z) \to 0$ as $z \to \infty$, we reject the roots with a positive real part. With the radicand of Eq. (13)

GMDD
8, 2847–2873, 2015

expressed in polar form, the physically acceptable roots are

$$M_0 = -\sqrt{k^2 + \frac{N^{2/3}k^{2/3}}{\nu^{1/3}\alpha^{1/3}}}, \quad (n=0), \tag{14a}$$

$$M_1 = -r^{1/2}e^{i\phi/2}, \quad (n=1), \tag{14b}$$

$$M_2 = -r^{1/2}e^{-i\phi/2}, \quad (n=2), \tag{14c}$$

where the subscript on M denotes the associated value of n, and r and ϕ are defined by

$$r \equiv \sqrt{\left[k^2 + \frac{N^{2/3}k^{2/3}}{\nu^{1/3}\alpha^{1/3}}\cos\left(\frac{2\pi}{3}\right)\right]^2 + \left[\frac{N^{2/3}k^{2/3}}{\nu^{1/3}\alpha^{1/3}}\sin\left(\frac{2\pi}{3}\right)\right]^2}, \tag{15}$$

$$\cos\phi = \frac{1}{r}\left[k^2 + \frac{N^{2/3}k^{2/3}}{\nu^{1/3}\alpha^{1/3}}\cos\left(\frac{2\pi}{3}\right)\right], \quad \sin\phi = \frac{1}{r}\left(\frac{N^{2/3}k^{2/3}}{\nu^{1/3}\alpha^{1/3}}\right)\sin\left(\frac{2\pi}{3}\right) > 0. \tag{16}$$

When solving Eq. (16) for ϕ, care must be taken when evaluating arcsin or arccos functions that ϕ appears in the correct quadrant (ϕ should be in quadrant I or II so $\phi/2$ should always be in quadrant I). Also note from Eqs. (14b) and (14c) that M_2 is the complex conjugate of M_1 ($M_2 = M_1^*$), a fact that will often be used below.

With the general solution for ψ written as

$$\psi = (Be^{M_0 z} + Ce^{M_1 z} + De^{M_2 z})\cos kx, \tag{17}$$

where B, C, and D are constants, the vorticity becomes,

$$\eta = \left[B(M_0^2 - k^2)e^{M_0 z} + C(M_1^2 - k^2)e^{M_1 z} + D(M_2^2 - k^2)e^{M_2 z}\right]\cos kx, \tag{18}$$

and the buoyancy follows from Eq. (3) as

$$b = \frac{kN^2}{\alpha}\left(\frac{B}{M_0^2 - k^2}e^{M_0 z} + \frac{C}{M_1^2 - k^2}e^{M_1 z} + \frac{D}{M_2^2 - k^2}e^{M_2 z}\right)\sin kx + b_h, \tag{19}$$

GMDD
8, 2847–2873, 2015

where $\nabla^2 b_h = 0$. In view of Eq. (12), Eq. (19) becomes

$$b = \frac{k^{1/3}\nu^{1/3}N^{4/3}}{\alpha^{2/3}}(Be^{M_0 z} + e^{-2\pi i/3}Ce^{M_1 z} + e^{-4\pi i/3}De^{M_2 z})\sin kx + b_h. \quad (20)$$

Applying Eqs. (18) and (20) in Eq. (5) yields an equation for $\partial b_h/\partial x$, which upon use of Eq. (12) and $M_2 = M_1^*$ reduces to $\partial b_h/\partial x = 0$. So b_h is, at most, a function of z. Since $\nabla^2 b_h = 0$, b_h is, at most, a linear function of z, and since b should vanish as $z \to \infty$, that linear function must be 0. Thus, $b_h = 0$.

The pressure follows from Eqs. (1) and (12) as

$$\Pi = \frac{\nu^{2/3}N^{2/3}}{k^{1/3}\alpha^{1/3}}(BM_0 e^{M_0 z} + CM_1 e^{2\pi i/3}e^{M_1 z} + DM_2 e^{4\pi i/3}e^{M_2 z})\sin kx + G(z), \quad (21)$$

where $G(z)$ is a function of integration. Applying Eq. (21) in Eq. (2), and using Eq. (11) yields $\mathrm{d}G/\mathrm{d}z = 0$, so G is constant. For Π to vanish as $z \to \infty$, this constant must be zero.

The surface conditions determine B, C, and D. The surface buoyancy is

$$b(x, 0) = b_0 \sin kx, \quad (22)$$

where b_0 is a constant forcing amplitude. Application of Eq. (20) in Eq. (22) yields

$$B + e^{-2\pi i/3}C + e^{-4\pi i/3}D = \frac{b_0\alpha^{2/3}}{k^{1/3}\nu^{1/3}N^{4/3}}. \quad (23)$$

The impermeability and no-slip conditions yield

$$B + C + D = 0, \quad (24)$$

$$BM_0 + CM_1 + DM_2 = 0. \quad (25)$$

GMDD
8, 2847–2873, 2015

Straightforward but lengthy manipulations yield the solution of Eqs. (23)–(25):

$$B = -\left(\frac{b_0\alpha^{2/3}}{\sqrt{3}k^{1/3}\nu^{1/3}N^{4/3}}\right)\frac{2r^{1/2}\sin(\phi/2)}{M_0 + 2r^{1/2}\cos(\pi/3+\phi/2)}, \tag{26}$$

$$C = -i\left(\frac{b_0\alpha^{2/3}}{\sqrt{3}k^{1/3}\nu^{1/3}N^{4/3}}\right)\frac{M_2 - M_0}{M_0 + 2r^{1/2}\cos(\pi/3+\phi/2)}, \tag{27}$$

$$D = i\left(\frac{b_0\alpha^{2/3}}{\sqrt{3}k^{1/3}\nu^{1/3}N^{4/3}}\right)\frac{M_1 - M_0}{M_0 + 2r^{1/2}\cos(\pi/3+\phi/2)}. \tag{28}$$

Applying Eqs. (26)–(28) in Eqs. (17), (20), and (18), with Eq. (12) used in the latter equation, and noting that B is real, while $D = C^*$ (since $M_2 = M_1^*$), we obtain

$$b = \frac{2b_0}{\sqrt{3}}\frac{e^{-Z_c}[\mu\cos(Z_s+\pi/6)+\cos(Z_s+\pi/6+\phi/2)] - e^{M_0 z}\sin(\phi/2)}{\mu + 2\cos(\pi/3+\phi/2)}\sin kx, \tag{29}$$

$$\psi = \frac{2b_0\alpha^{2/3}}{\sqrt{3}k^{1/3}\nu^{1/3}N^{4/3}}\frac{e^{-Z_c}[\mu\sin Z_s+\sin(Z_s+\phi/2)] - e^{M_0 z}\sin(\phi/2)}{\mu + 2\cos(\pi/3+\phi/2)}\cos kx, \tag{30}$$

where

$$Z_s \equiv zr^{1/2}\sin(\phi/2), \quad Z_c \equiv zr^{1/2}\cos(\phi/2), \quad \mu \equiv M_0/r^{1/2}. \tag{31}$$

The vertical velocity follows from Eq. (30) as

$$w = \frac{2b_0\alpha^{2/3}k^{2/3}}{\sqrt{3}\nu^{1/3}N^{4/3}}\frac{e^{-Z_c}[\mu\sin Z_s+\sin(Z_s+\phi/2)] - e^{M_0 z}\sin(\phi/2)}{\mu + 2\cos(\pi/3+\phi/2)}\sin kx. \tag{32}$$

GMDD
8, 2847–2873, 2015

2.3 Piecewise constant (square wave) forcing

Next, consider the case where the surface buoyancy varies horizontally as a square wave, with a distribution over one period L given by,

$$b(x,0) = \begin{cases} b_{\max}, & 0 < x < L/2, \\ -b_{\max}, & L/2 < x < L. \end{cases} \tag{33}$$

Such a distribution can be expressed as the Fourier series,

$$b(x,0) = \sum_{n=1}^{\infty} b_n \sin\left(\frac{n\pi x}{L}\right), \tag{34}$$

$$b_n = \frac{2}{L}\int_0^L b(x,0)\sin\left(\frac{n\pi x}{L}\right). \tag{35}$$

Application of Eq. (33) in Eq. (35) yields

$$b_n = \frac{2b_{\max}}{n\pi}\left[1 - 2\cos(n\pi/2) + \cos(n\pi)\right]. \tag{36}$$

The solutions for b, ψ, and w can then be written as summations over the single-harmonic solutions Eqs. (29), (30), and (32), with k related to n by

$$k = \frac{n\pi}{L}, \tag{37}$$

GMDD
8, 2847–2873, 2015

and with b_0 replaced by b_n:

$$b = \frac{2}{\sqrt{3}} \sum_{n=1}^{\infty} b_n \frac{e^{-Z_c}[\mu \cos(Z_s + \pi/6) + \cos(Z_s + \pi/6 + \phi/2)] - e^{M_0 z} \sin(\phi/2)}{\mu + 2\cos(\pi/3 + \phi/2)} \cdot \sin\left(\frac{n\pi x}{L}\right), \tag{38}$$

$$\psi = \frac{2\alpha^{2/3}}{\sqrt{3} k^{1/3} \nu^{1/3} N^{4/3}} \sum_{n=1}^{\infty} b_n \frac{e^{-Z_c}[\mu \sin Z_s + \sin(Z_s + \phi/2)] - e^{M_0 z} \sin(\phi/2)}{\mu + 2\cos(\pi/3 + \phi/2)} \cdot \cos\left(\frac{n\pi x}{L}\right), \tag{39}$$

$$w = \frac{2\alpha^{2/3} k^{2/3}}{\sqrt{3} \nu^{1/3} N^{4/3}} \sum_{n=1}^{\infty} b_n \frac{e^{-Z_c}[\mu \sin Z_s + \sin(Z_s + \phi/2)] - e^{M_0 z} \sin(\phi/2)}{\mu + 2\cos(\pi/3 + \phi/2)} \sin\left(\frac{n\pi x}{L}\right). \tag{40}$$

The derivation of the u field requires considerable effort and is not pursued. Instead, we obtain a proxy of the analytical solution for u by taking centered finite differences of Eq. (39) with respect to z.

3 Verification tests

A solution of the linearized equations may be used to verify a nonlinear code if the nonlinear terms are sufficiently small. Unfortunately, a priori estimates of such terms expressed, for example, through a Reynolds number, are not straightforward since the relevant velocity and length scales in our problem are only evident after a solution has been obtained. We thus seek an appropriate set of test parameters through trial and error, guided by a posteriori linear solution estimates of the terms $\boldsymbol{u} \cdot \nabla b$ and $\boldsymbol{u} \cdot \nabla \eta$ present in nonlinear versions of Eqs. (3) and (5), respectively. Specifically, for any computed candidate solution, we formed the ratios of the largest values of those nonlinear

GMDD
8, 2847–2873, 2015

terms to the largest values of the corresponding linear terms, that is, the terms actually present in Eqs. (3) and (5). We need only consider one such linear term per ratio since Eqs. (3) and (5) are comprised of two terms of equal magnitude. A solution was deemed to be sufficiently linear if

$$R_\eta \equiv \frac{\max|\boldsymbol{u}\cdot\nabla\eta|}{\max\left|\partial b/\partial x\right|} < \varepsilon, \quad \text{and} \quad R_b \equiv \frac{\max|\boldsymbol{u}\cdot\nabla b|}{\max|\alpha\nabla^2 b|} < \varepsilon, \tag{41}$$

where ε ($\ll 1$) is a prescribed threshold. The suitability of this approach was confirmed by the very close agreement between the analytical solutions and the numerical solutions obtained with the correct surface pressure condition.

The numerical model employed in our tests is a variant of a direct numerical simulation (DNS) code used in the boundary-layer and slope-flow studies of Fedorovich et al. (2001), Fedorovich and Shapiro (2009a, b), and Shapiro and Fedorovich (2013, 2014). The model solves the Boussinesq governing equations on an Arakawa C grid. Although designed for three-dimensional simulations, the model was run in a two-dimensional (x, z) mode. The overall solution procedure is patterned on a fractional step method proposed by Chorin (1968). In our version, the prognostic equations are integrated using a filtered leapfrog scheme with explicit treatment of the viscous term. The pressure is diagnosed from a Poisson equation, which is solved using a fast Fourier transform technique in horizontal planes, and a tridiagonal matrix inversion in the vertical. The surface condition on pressure is the inhomogeneous Neumann condition that arises from projecting the vertical equation of motion into the vertical, and imposing the impermeability condition (Vreman, 2014; also see our Appendix). We also run a version of the code in which the surface pressure condition is mis-specified as a homogeneous Neumann condition. We hasten to add, however, that our implementation of the homogeneous condition may be quite different from implementations described in the literature. We elaborate on these technical differences and review general aspects of the problem of surface pressure specification in the Appendix.

GMDD
8, 2847–2873, 2015

The analytical solution was evaluated on an un-staggered (x, z) grid extending over one period of the square wave ($x = 0$ to $x = L$). The series were truncated at 50 000 terms. The governing parameters were adjusted so that the linearity criteria were satisfied in comparisons with $\varepsilon = 5 \times 10^{-3}$.

In the first test, we set $\nu = \alpha = 0.001\,\mathrm{m^2\,s^{-1}}$, $N = 0.02\,\mathrm{s^{-1}}$, $L = 5.12\,\mathrm{m}$, and $b_{\max} = 1 \times 10^{-5}\,\mathrm{m\,s^{-2}}$. For the analytical solution A-1, the (x, z) grid consisted of 513×1025 points with grid spacings $\Delta x = \Delta z = 0.01\,\mathrm{m}$. The linearity criteria Eq. (41) were satisfied with $R_\eta \cong 8.2 \times 10^{-5}$ and $R_b \cong 2.8 \times 10^{-3}$. The analytical b and w fields shown in Fig. 2 depict a broad zone of ascent above the warm surface and a compensating zone of descent over the cold surface, roughly for $z < 1.8\,\mathrm{m}$. In the upper part of these zones (roughly $0.9\,\mathrm{m} < z < 1.8\,\mathrm{m}$), adiabatic expansion/compression has reversed the senses of the buoyancy fields. Surprisingly, the numerical fields in the inhomogeneous INC-1 and homogeneous HNC-1 cases are very similar to each other and to the A-1 fields. The u fields from A-1, INC-1, and HNC-1 shown in Fig. 3 are visually indistinguishable from one another.

To understand why the INC-1 and HNC-1 simulations are so similar, and to identify simulation parameters that might evince more substantial differences, we consider the idealized problem in which a specified buoyancy $b = b_0 e^{-\gamma z} \sin kx$ ($\gamma = h^{-1}$, where h is the e-folding depth scale) is the only forcing term in the Poisson equation $\nabla^2 \Pi = \partial b / \partial z$ with Neumann surface condition $\partial \Pi / \partial z \big|_0 = b(x, 0)$. This idealized problem is solved as

$$\Pi^*_{\mathrm{INC}} = \frac{b_0}{\gamma^2 - k^2} \left(k e^{-kz} - \gamma e^{-\gamma z} \right) \sin kx. \tag{42}$$

The corresponding solution obtained with the homogeneous Neumann condition, $\partial \Pi / \partial z \big|_0 = 0$, is

$$\Pi^*_{\mathrm{HNC}} = \frac{b_0}{\gamma^2 - k^2} \left(\frac{\gamma^2}{k} e^{-kz} - \gamma e^{-\gamma z} \right) \sin kx. \tag{43}$$

GMDD
8, 2847–2873, 2015

The relative error (RE) in the vertical pressure gradient force associated with Eqs. (42) and (43), defined as the local absolute error in that force divided by the local buoyancy, is calculated as

$$\mathrm{RE} \equiv \left| \frac{\partial \Pi^*_{\mathrm{INC}}/\partial z - \partial \Pi^*_{\mathrm{HNC}}/\partial z}{b} \right| = e^{(a-1)kz}, \tag{44}$$

where $a \equiv \gamma/k$. Written in terms of the depth scale h and wavelength $\lambda = 2\pi/k$, a can be interpreted as an aspect ratio characterizing the width to depth scales of the disturbance, $a = \lambda/(2\pi h) \propto \lambda\gamma$. From Eq. (44) we see that RE decreases exponentially with z for disturbances characterized by small aspect ratios, $a < 1$ (which we refer to as deep disturbances) and increases exponentially with z for disturbances characterized by large aspect ratios, $a > 1$ (which we refer to as shallow disturbances). The buoyancy in Fig. 2 is suggestive of $a < 1$, which indicates that the first test could be classified as a deep (error-forgiving) simulation.

The preceding analysis suggests that simulations with shallow thermal disturbances ($a > 1$) might yield large differences between cases with inhomogeneous and homogeneous Neumann conditions. There did not appear to be a straightforward way to increase the effective a by systematically varying the parameters (e.g., increasing L tended to increase the effective h), but a set of suitable parameters were identified through trial and error and were used as the basis for the second test case.

In the second test, we set $\nu = \alpha = 0.0001\,\mathrm{m^2\,s^{-1}}$, $N = 0.2\,\mathrm{s^{-1}}$, $L = 10.24\,\mathrm{m}$, and $b_{\max} = 5\times10^{-6}\,\mathrm{m\,s^{-2}}$. The analytical solution A-2 was generated with 2049×513 points with grid spacings of $\Delta x = \Delta z = 0.005\,\mathrm{m}$. The linearity criteria were satisfied with $R_\eta \cong 4.8\times10^{-5}$ and $R_b \cong 3.6\times10^{-3}$. In contrast to the counter-rotating convection rolls seen in the first test, the analytical b and w fields shown in Fig. 4 depict narrow updraft/downdraft pairs straddling the buoyancy discontinuities. Between the narrow updrafts is a broad region of relatively weak ascent. The w and b fields above the cold surface are mirror images of the fields above the warm surface. Note the change in the scales of the x and (especially) the z axes between Figs. 4 and 2: the low-level

GMDD
8, 2847–2873, 2015

thermal disturbance in the second test is much shallower than the disturbance in the first test (and is suggestive of $a > 1$). In this second test case we find dramatic differences between the inhomogeneous INC-2 and homogeneous HNC-2 cases. Specifically, while the INC-2 and A-2 fields are in excellent agreement, the HNC-2 fields showed no signs of even approaching a steady state. Long after the INC-2 simulation had reached a steady state, the HNC-2 fields continued to amplify and develop asymmetric structures associated with flow nonlinearities. The very close agreement between the A-2 solution and the steady state in the INC-2 simulation is shown for the u field in Fig. 5. The u field in the disastrous HNC-2 simulation, at a time when a steady state had already been attained in the INC-2 simulation, is shown in Fig. 6.

4 Summary

The linearized Boussinesq equations for the motion of a viscous stably stratified fluid are solved analytically for a surface buoyancy that varies laterally as a square wave. The solution describes two-dimensional laminar convective structures such as thermal convective rolls and updraft/downdraft pairs. The main applications of the solution may be in code verification and the evaluation of different implementations of the surface pressure condition for the pressure Poisson equation. Tests have been conducted for cases where the aspect ratios of the thermal disturbance have been large and small. With attention restricted to disturbances of sufficiently small amplitude, the linear solution and numerically simulated fields with the inhomogeneous Neumann condition for pressure (which is appropriate in the context of the particular fractional step procedure adopted in our DNS code) have been found to be in excellent agreement for both tests. However, in tests with a mis-specified Neumann condition, an excellent agreement with the analytical solution has been found only for the deep (small aspect ratio) disturbance case; errors in the shallow (large aspect ratio) disturbance case have been catastrophic.

GMDD
8, 2847–2873, 2015

Appendix A: Comment on the pressure condition at a lower solid surface

Consider a Boussinesq system with equation of motion,

$$\frac{\partial \boldsymbol{u}}{\partial t} = -\nabla \Pi + \nu \nabla^2 \boldsymbol{u} + \mathbf{F}. \tag{A1}$$

Here $\boldsymbol{u}$ is the velocity vector, Π is a kinematic pressure perturbation, ν is the kinematic viscosity coefficient, and $\mathbf{F}$ is the sum of nonlinear acceleration and buoyancy terms. Applying the incompressibility condition,

$$\nabla \cdot \boldsymbol{u} = 0, \tag{A2}$$

in the equation that results from taking the divergence of Eq. (A1) (e.g., Orszag et al., 1986) yields the Poisson equation,

$$\nabla^2 \Pi = \nabla \cdot \mathbf{F}. \tag{A3a}$$

Although Eqs. (A1) and (A2) imply Eq. (A3a), the reverse statement is not generally true. Indeed, eliminating Π from between Eq. (A3a) and the equation arising from taking the divergence of Eq. (A1) yields the diffusion equation $\partial \delta / \partial t = \nu \nabla^2 \delta$ for the velocity divergence $\delta \equiv \nabla \cdot \boldsymbol{u}$, whose solution is Eq. (A2) only if $\nabla \cdot \boldsymbol{u}$ is zero initially and on all boundaries (Orszag et al., 1986; Gresho and Sani, 1987).

The same steps leading to Eq. (A3a) also lead to an alternative Poisson equation,

$$\nabla^2 \Pi = \nabla \cdot \left(\nu \nabla^2 \boldsymbol{u} + \mathbf{F} \right). \tag{A3b}$$

Although $\nabla \cdot \nu \nabla^2 \boldsymbol{u}$ was omitted in Eq. (A3a) [this term is zero if Eq. (A2) is satisfied], Gresho and Sani (1987) advocate its retention: "If you include it, you don't need it; if you don't include it, you need it." Equation (A3b) is the form adopted in our numerical code.

GMDD
8, 2847–2873, 2015

Evaluating the vertical component of Eq. (A1) on the surface, where the impermeability condition applies, yields the inhomogeneous Neumann condition,

$$\left.\frac{\partial \Pi}{\partial z}\right|_0 = \nu \left.\frac{\partial^2 w}{\partial z^2}\right|_0 + F_z|_0, \tag{A4}$$

where $w \equiv \boldsymbol{k}\cdot\boldsymbol{u}$, $F_z \equiv \boldsymbol{k}\cdot\mathbf{F}$, $\boldsymbol{k}$ is the upward unit vector, and $()|_0$ is a surface value. It has been argued that Eq. (A4), by itself, is not a proper boundary condition because it does not provide new information (as it is not independent of the governing equations) and does not enforce the incompressibility condition Eq. (A2) at the boundary (Strikwerda, 1984; Henshaw, 1994; Sani et al., 2006). However, as pointed out by Henshaw (1994), many studies that impose Eq. (A4) (or a variant of it) also apply Eq. (A2) on the boundary.

In our numerical model, Eq. (A1) is integrated using a fractional step procedure with explicit treatment of the viscous term. First, a provisional velocity field $\widetilde{\boldsymbol{u}}$ that does not satisfy Eq. (A2) is obtained by integrating a discretized form of Eq. (A1) in which the pressure gradient is omitted. The provisional velocity is equal to the velocity at the end of the previous time step plus the sum of the forcing terms (nonlinear acceleration, buoyancy, and viscous stress) multiplied by the time step δt. With the forcing terms explicitly evaluated, $\widetilde{\boldsymbol{u}}$ is readily computed throughout the flow domain, including on the surface, where, in surface-forced flows, the buoyancy will make a substantial contribution. In terms of $\widetilde{\boldsymbol{u}}$ and its vertical component $\widetilde{w}$, Eqs. (A3b) and (A4) become,

$$\nabla^2 \Pi = \frac{\nabla\cdot\widetilde{\boldsymbol{u}}}{\delta t}, \tag{A5}$$

$$\left.\frac{\partial \Pi}{\partial z}\right|_0 - \frac{1}{\delta t}\widetilde{w}|_0 = 0. \tag{A6}$$

In the second step, a velocity field that does satisfy Eq. (A2) is obtained by solving Eq. (A5), and then adding the pressure gradient force associated with this Π (multiplied by δt) to $\widetilde{\boldsymbol{u}}$.

GMDD
8, 2847–2873, 2015

In some explicit fractional step procedures (including the DNS code used in our study), the problem of solving Eq. (A5) subject to Eq. (A6) with $\widetilde{\boldsymbol{u}}|_0$ evaluated from model data is replaced by what appears to be an entirely different (but is actually equivalent) problem: solving Eq. (A5) subject to the homogeneous Neumann condition,

$$\left.\frac{\partial \Pi}{\partial z}\right|_0 = 0, \tag{A7}$$

in concert with $\widetilde{\boldsymbol{u}}|_0$ being set to 0, obviating the need to calculate $\widetilde{\boldsymbol{u}}|_0$ from model data. It can be shown that $\widetilde{w}|_0$ and the discretized form of $\partial\Pi/\partial z\big|_0$ appear in the discretized form of Eq. (A5) valid half a grid point above the physical surface as $\partial\Pi/\partial z\big|_0 - \widetilde{w}|_0/\delta t$, that is, in the same combination as they appear in Eq. (A6). Thus, setting $\widetilde{w}|_0$ and $\partial\Pi/\partial z\big|_0$ to 0, is equivalent to implementing Eq. (A6) with the model-computed values of $\widetilde{w}|_0$: the discretized form of Eq. (A5) near the surface is the same in either case. Moreover, on the C grid, setting the tangential components $\widetilde{u}|_0$ and $\widetilde{v}|_0$ to 0 only affects the values of $\widetilde{u}$ and $\widetilde{v}$ half a grid point beneath the physical boundary. These values do not appear in the discretized form of Eq. (A5) at any z level, and thus have no bearing on the solution. In essence, the errors associated with the conflation of the two physically unjustifiable specifications (homogeneous Neumann condition for pressure, and $\widetilde{\boldsymbol{u}}|_0 = 0$) cancel out. The homogeneous Neumann condition for pressure can be the source of confusion if the context in which the condition is applied is not made clear: it would be a correct condition if $\widetilde{\boldsymbol{u}}|_0$ is set to zero (per the equivalence described above), but it would be an incorrect condition if the explicit model-computed values of $\widetilde{\boldsymbol{u}}|_0$ are used. In the experiments with the mis-specified condition described in Sect. 3, the homogeneous condition is imposed in the latter context. Unfortunately, in many numerical model descriptions, the nature of the surface pressure condition is left vague, for example, by not indicating whether a Neumann condition is homogeneous or inhomogeneous, or, if a homogeneous Neumann condition is indicated, not mentioning how $\widetilde{\boldsymbol{u}}|_0$ is treated.

GMDD
8, 2847–2873, 2015

Finally, we note that in fractional step procedures that treat the viscous term implicitly (e.g., Kim and Moin, 1985; Gresho, 1990; Armfield and Street, 2002; Guermond et al., 2006, and many others), the homogeneous Neumann condition is often applied as a surface condition for a Poisson equation, but it is again different from our implementation described in Sect. 3. In the implicit treatments, the provisional velocity is obtained as the solution of a boundary value problem ($\widetilde{\boldsymbol{u}}|_0$ should be specified; often it is set to 0) in which the relevant Poisson equation resembles Eq. (A5) but applies to a scalar function (sometimes called a pseudo-pressure) that is not the real pressure. Temam (1991) refers to this scalar as, "... a technical quantity, a mathematical auxiliary ..." and advocates that it should not even be considered as an approximation of the pressure. Interestingly, in the context of implicit treatments, the homogeneous Neumann condition on the pseudo-pressure has sometimes been implicated as corrupting solution accuracy through the development of spurious numerical boundary layers adjacent to solid boundaries (Gresho, 1990; Guermond et al., 2006; Hosseini and Feng, 2011).

Acknowledgements. This research was supported by the National Science Foundation under Grant AGS-1359698. Discussions with Chiel van Heerwaarden, Juan Pedro Mellado, and Inanc Senocak are gratefully acknowledged.

References

Armfield, S. and Street, R.: An analysis and comparison of the time accuracy of fractional-step methods for the Navier–Stokes equations on staggered grids, Int. J. Numer. Methods Fluids, 38, 255–282, 2002.

Atkinson, B.: Meso-Scale Atmospheric Circulations, Academic Press, 495 pp., 1981.

Axelsen, S. L., Shapiro, A., and Fedorovich, E.: Analytical solution for katabatic flow induced by an isolated cold strip, Environ. Fluid Mech., 10, 387–414, 2010.

Briggs, G. A.: Surface inhomogeneity effects on convective diffusion, Bound.-Lay. Meteorol., 45, 117–135, 1988.

GMDD

8, 2847–2873, 2015

Chorin, A. J.: Numerical solution of the Navier–Stokes equations, Math. Comput., 22, 745–762, 1968.
Fedorovich, E. and Shapiro, A.: Structure of numerically simulated katabatic and anabatic flows along steep slopes, Acta Geophys., 57, 981–1010, 2009a.
Fedorovich, E. and Shapiro, A.: Turbulent natural convection along a vertical plate immersed in a stably stratified fluid, J. Fluid Mech., 636, 41–57, 2009b.
Fedorovich, E., Nieuwstadt, F. T. M., and Kaiser, R.: Numerical and laboratory study of a horizontally evolving convective boundary layer. Part I: Transition regimes and development of the mixed layer, J. Atmos. Sci., 58, 70–86, 2001.
Gresho, P. M.: On the theory of semi-implicit projection methods for viscous incompressible flow and its implementation via a finite element method that also introduces a nearly consistent mass matrix. Part 1: Theory, Int. J. Numer. Methods Fluids, 11, 587–620, 1990.
Gresho, P. M. and Sani, R. L.: On pressure boundary conditions for the incompressible Navier–Stokes equations, Int. J. Numer. Methods Fluids, 7, 1111–1145, 1987.
Guermond, J. L., Minev, P., and Shen, J.: An overview of projection methods for incompressible flows, Comput. Methods Appl. Mech. Engrg., 195, 6011–6045, 2006.
Hadfield, M. G., Cotton, W. R., and Pielke, R. A.: Large-eddy simulations of thermally forced circulations in the convective boundary layer. Part I: A small-scale circulation with zero wind, Bound.-Lay. Meteorol., 57, 79–114, 1991.
Henshaw, W. D.: A fourth-order accurate method for the incompressible Navier–Stokes equations on overlapping grids, J. Comput. Phys., 113, 13–25, 1994.
Hosseini, S. M. and Feng, J. J.: Pressure boundary conditions for computing incompressible flows with SPH, J. Comput. Phys., 230, 7473–7487, 2011.
Kang, S.-L., Lenschow, D., and Sullivan, P.: Effects of mesoscale surface thermal heterogeneity on low-level horizontal wind speeds, Bound.-Lay. Meteorol., 143, 409–432, 2012.
Kim, J. and Moin, P.: Application of a fractional-step method to incompressible Navier–Stokes equations, J. Comput. Phys., 59, 308–323, 1985.
Mahrt, L., Sun, J., Vickers, D., MacPherson, J. I., Pederson, J. R., and Desjardins, R. L.: Observations of fluxes and inland breezes over a heterogeneous surface, J. Atmos. Sci., 51, 2484–2499, 1994.
McPherson, R. A.: A review of vegetation-atmosphere interactions and their influences on mesoscale phenomena, Prog. Phys. Geog., 31, 261–285, 2007.

GMDD
8, 2847–2873, 2015

Nordström, J., Mattsson, K., and Swanson, C.: Boundary conditions for a divergence free velocity-pressure formulation of the Navier–Stokes equations, J. Comput. Phys., 225, 874–890, 2007.
Orszag, S. A., Israeli, M., and Deville, M. O.: Boundary conditions for incompressible flows, J. Sci. Comput., 1, 75–111, 1986.
Patton, E. G., Sullivan, P. P., and Moeng, C.-H.: The influence of idealized heterogeneity on wet and dry planetary boundary layers coupled to the land surface, J. Atmos. Sci., 62, 2078–2097, 2005.
Petersson, N. A.: Stability of pressure boundary conditions for Stokes and Navier–Stokes equations, J. Comput. Phys., 172, 40–70, 2001.
Pielke, R. A.: Influence of the spatial distribution of vegetation and soils on the prediction of cumulus convective rainfall, Rev. Geophys., 39, 151–177, 2001.
Rempfer, D.: On boundary conditions for incompressible Navier–Stokes problems, Appl. Mech. Rev., 59, 107–125, 2006.
Segal, M. and Arritt, R. W.: Non-classical mesoscale circulations caused by surface sensible heat-flux gradients, B. Am. Meteorol. Soc., 73, 1593–1604, 1992.
Shapiro, A. and Fedorovich, E.: Similarity models for unsteady free convection flows along a differentially cooled horizontal surface, J. Fluid Mech., 736, 444–463, 2013.
Shapiro, A. and Fedorovich, E.: A boundary-layer scaling for turbulent katabatic flow, Bound.-Lay. Meteorol., 153, 1–17, 2014.
Shirokoff, D. and Rosales, R. R.: An efficient method for the incompressible Navier–Stokes equations on irregular domains with no-slip boundary conditions, high order up to the boundary, J. Comput. Phys., 230, 8619–8646, 2011.
Simpson, J. E.: Sea Breeze and Local Winds, Cambridge University Press, 234 pp., 1994.
Temam, R.: Remark on the pressure boundary condition for the projection method, Theor. Comp. Fluid Dyn., 3, 181–184, 1991.
Strikwerda, J. C.: Finite difference methods for the Stokes and Navier–Stokes equations, SIAM J. Sci. Stat. Comp., 5, 56–68, 1984.
van Heerwaarden, C. C., Mellado, J. P., and de Lozar, A.: Scaling laws for the heterogeneously heated free convective boundary layer, J. Atmos. Sci., 71, 3975–4000, 2014.
Vreman, A. W.: The projection method for the incompressible Navier–Stokes equations: the pressure near a no-slip wall, J. Comput. Phys., 263, 353–374, 2014.

GMDD
8, 2847–2873, 2015

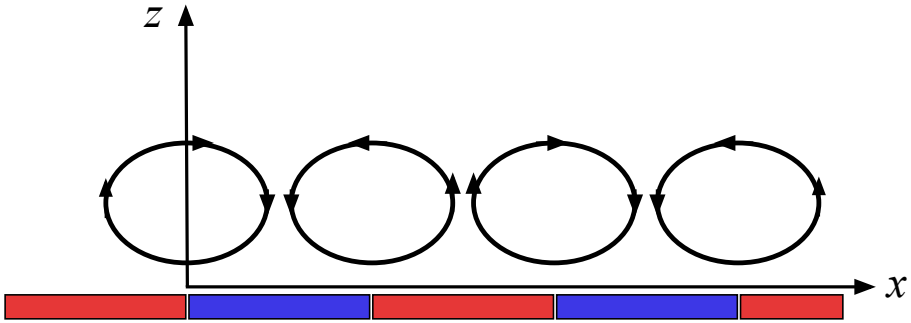

Figure 1. Schematic of two-dimensional (x, z) thermal convection induced by a surface buoyancy that varies horizontally (x) as a square wave. Red denotes positive surface buoyancy, blue denotes negative surface buoyancy.

GMDD
8, 2847–2873, 2015

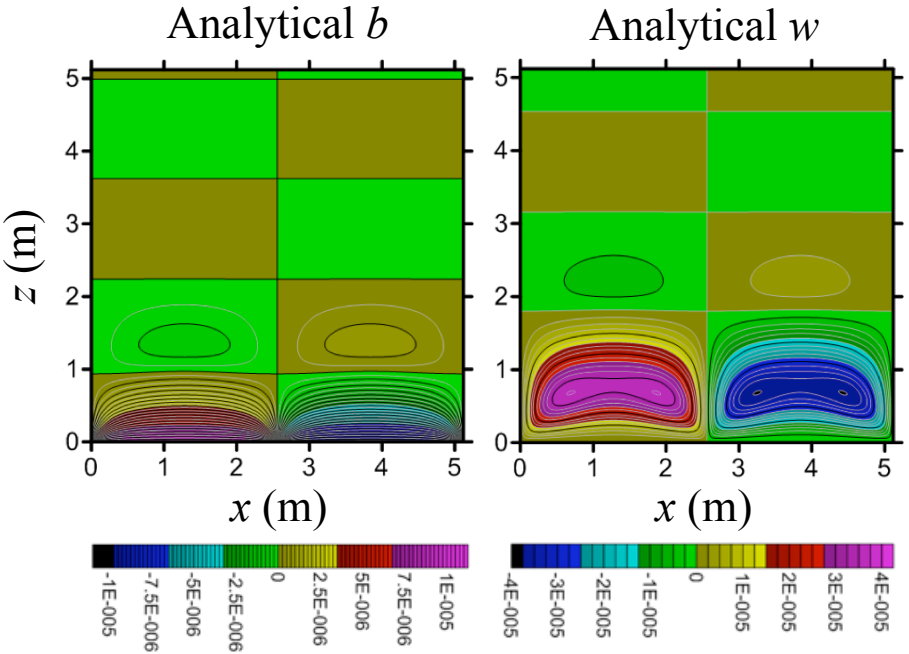

Figure 2. Vertical cross section of the analytical (A-1) buoyancy b and vertical velocity w fields from the first test case. Color bar units are $\mathrm{m\,s^{-2}}$ for b, and $\mathrm{m\,s^{-1}}$ for w.

GMDD
8, 2847–2873, 2015

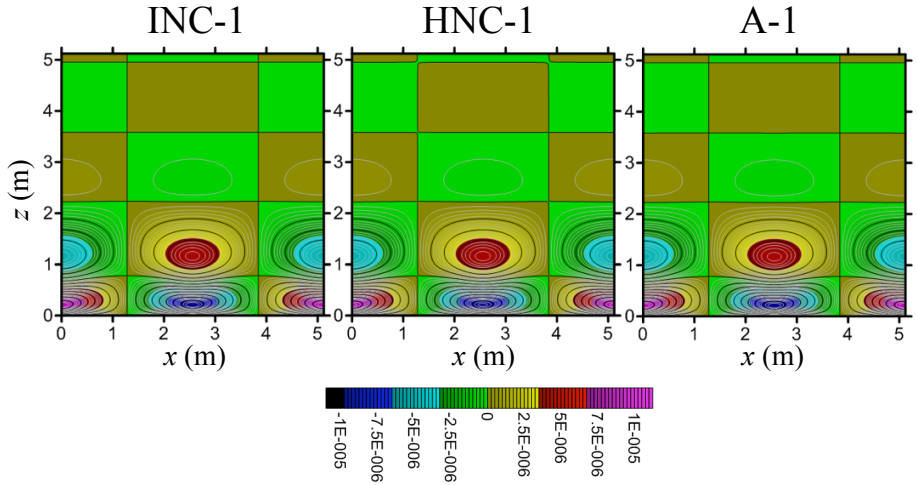

Figure 3. Vertical cross section of u from the first test case. A-1 is the analytical solution. INC-1 is the numerical simulation with inhomogeneous Neumann condition for pressure. HNC-1 is the numerical simulation with the homogeneous Neumann condition for pressure. Color bar units are $\mathrm{m\,s^{-1}}$.

GMDD
8, 2847–2873, 2015

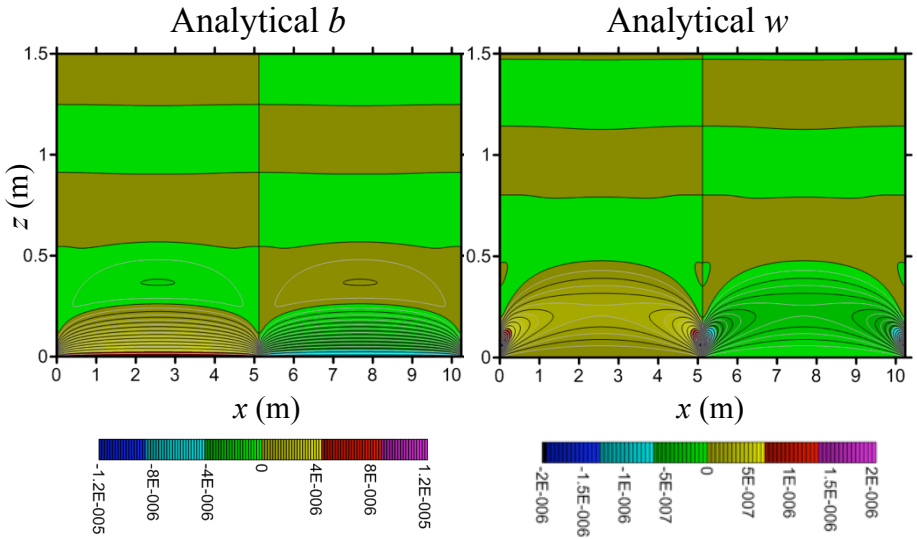

Figure 4. Vertical cross section of the analytical (A-2) buoyancy b and vertical velocity w fields from the second test case. Color bar units are $\mathrm{m\,s^{-2}}$ for b, and $\mathrm{m\,s^{-1}}$ for w.

GMDD
8, 2847–2873, 2015

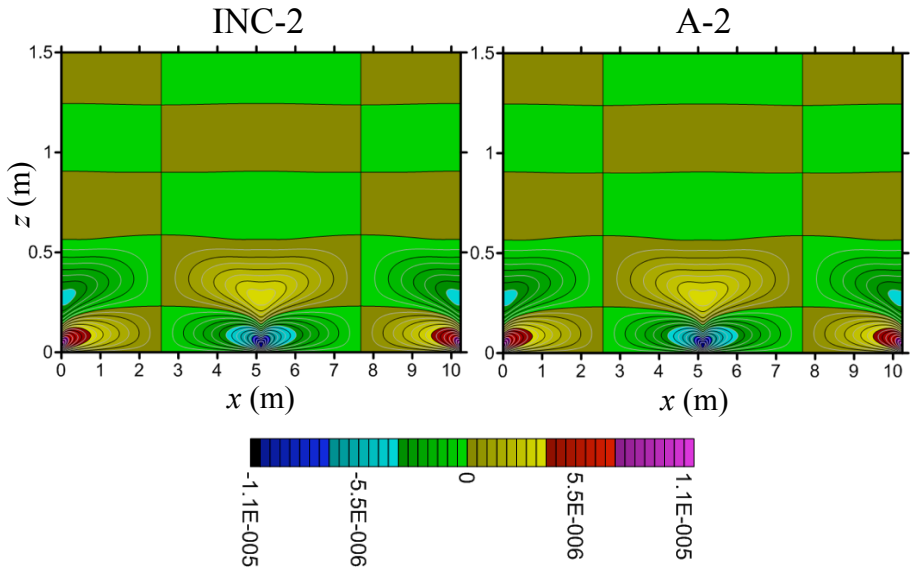

Figure 5. Vertical cross section of u from the second test case. A-2 is the analytical solution. INC-2 is the numerical simulation with inhomogeneous Neumann condition for pressure. Color bar units are $m s^{-1}$.

GMDD
8, 2847–2873, 2015

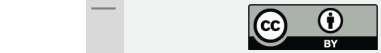

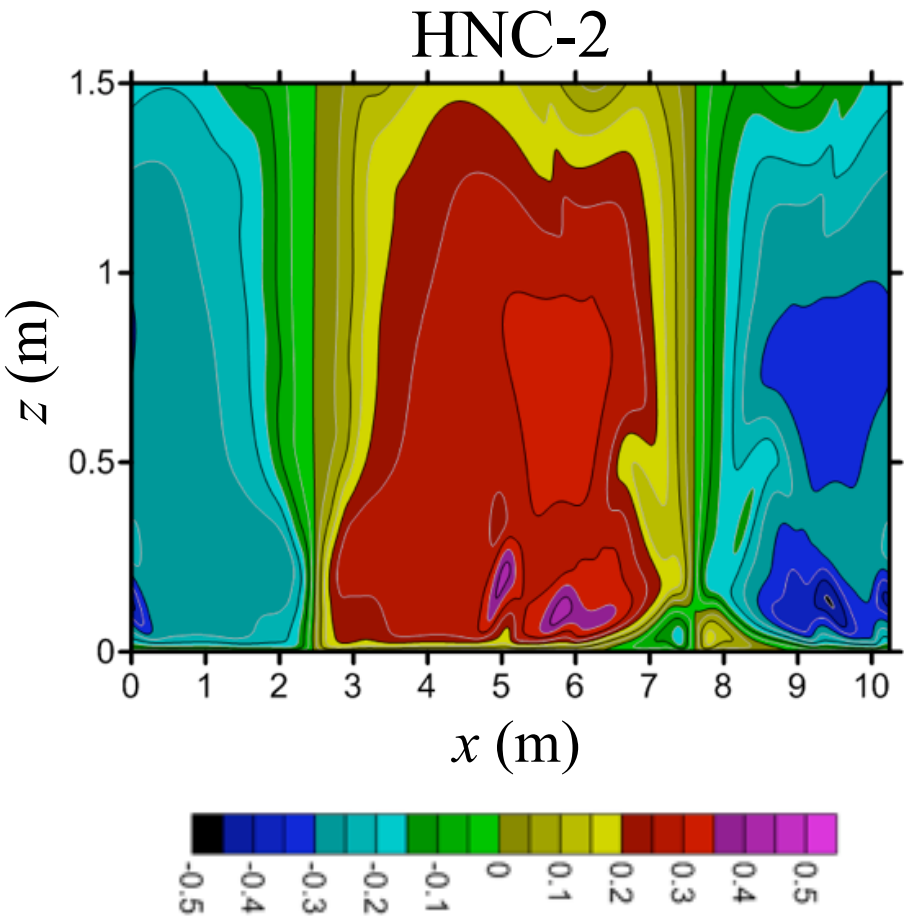

Figure 6. Vertical cross section of u from HNC-2, the numerical simulation with homogeneous Neumann condition for pressure in the second test case. Color bar units are $\mathrm{m\,s^{-1}}$.
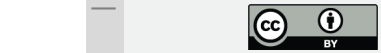
GMDD
8, 2847–2873, 2015